Generation and dynamics of one-, two- and three-dimensional cavity soliton in VCSEL with saturable absorber and frequency-selective feedback

BALDEEP KAUR[1] AND SOUMENDU JANA[1,*]

[1]*School of Physics and Materials Science, Thapar Institute of Engineering and Technology University, Patiala-147004, India*
[*]*Corresponding author: soumendu.jana@thapar.edu*

Cavity solitons are predicted in vertical-cavity surface emitting laser with a saturable absorber and coupled to an external frequency-selective feedback element. An entirely variational method based analytical study of the complex Ginzburg-Landau equation; the governing equation of the system, gives rise to one-, two- and three-dimensional cavity solitons. All three types of cavity solitons are verified stable by Lyapunov stability analysis. Stability regions are identified for all three types and are found to shrink with increasing dimensionality. Split-step Fourier method based direct numerical analysis of the governing equation exhibits matching results for existence and stability of the cavity solitons. Cavity soliton interaction has been studied numerically. All-optical control on cavity soliton has been demonstrated by introducing phase gradient. Cavity solitons thus generated have potential applications in optical information technology.

1. INTRODUCTION

From Scott Russell's 'wave of translation', soliton has come up to an age of on-chip photonics [1]. Cavity solitons (CS) are an important constituent in realizing such wafer level photonic devices. CS belongs to a unique class of spatial optical dissipative solitons, observed in broad-area systems far from an equilibrium [2, 3]. They are self-localized, non-diffracting and self-organized optical structures observed in dissipative optical cavities with gain and absorption, driven by a holding beam or an optical feedback element. CS shares some properties of spatial dissipative solitons, however, their exponential confinement, plasticity (freedom of occurrence at any point on a plane transverse to cavity axis) and bistability (being 'on' and 'off' at the same condition) made them unique [4]. From the point of pattern formation, CSs are localized pattern state over a co-existing stable homogeneous background state. The localized pattern formation is best observed in a spatially extended system like a vertical-cavity surface emitting laser (VCSEL). For investigating generation and dynamics of CS a VCSEL is usually preferred over edge emitters due to its several advantages like long device lifetime, single mode operation, low threshold current, lasing wavelength stability, high efficiency, symmetry of emitted beam profile and high temperature operations (usually 80°C). The basic structure of VCSEL consists of semiconductor

micro-cavity, closed by highly reflective distributed Bragg reflectors (DBR). Typically, cavity thickness is of the order of one wavelength while the effective cavity length can be upto 1-2 μm, with aperture size of 100-200 μm and an approximate emission wavelength of 981 nm at an operating temperature of 80°C [1, 5]. The large transverse area of VCSEL facilitates the observation of the localized pattern, hence CS and its dynamics. Ring resonator cavity, single-mirror feedback cavity, double-mirror feedback are some of the commonly available cavity schemes. Among them, owing to the minimum configuration and simplicity of working, a single-mirror feedback serves the purpose to its best [1]. The localization and hence spatial (temporal) soliton formation in conservative system requires the balance between self-diffraction (group velocity dispersion) and nonlinearity induced self-focusing (self-phase modulation). Fulfilling this still leaves a condition due in achieving localization in a dissipative system. It is the loss-gain balance. [6]. Due to this requirement of 'two-fold' balances CS appears as fixed points or only in a finite narrow range of parameters, usually, referred as pinning region. Several experimental schemes have been used to generate CS in VCSEL. Generally, holding beam is coupled with VCSEL for providing the continuous power to keep CS 'live'. A simpler but better scheme is an external feedback, for example, a frequency-selective feedback (FSF) element coupled with a

VCSEL [7]. The presence of feedback eliminates the need of holding beam and undesired thermal effects and other concomitant complicacies arising due to it [7, 8]. A significant volume of work [1, 4, 5, 9–12] has been reported on theoretical as well as experimental investigation of CS and cavity soliton laser (CSL) with FSF. Saturable absorber (SA) may also replace the holding beam. SA involves higher order nonlinearities that facilitate in achieving stability of the CS system. Materials with higher order nonlinearities like some semiconductors [13] and organic materials [14] can be used as dopents to form SA. Seminal works by Goldstone [15] and Rozanov *et al.* [16–19] have predicted both analytical as well as numerical existence of CS in VCSEL with SA. Subsequently, the existence of CS is analytically demonstrated with SA [1] and references therein. Although, a VCSEL coupled with FSF is considered as an advantageous scheme for CS formation it still lacks the bistability between lasing and non-lasing states. The same can be obtained by inclusion of SA in laser cavity [1, 8]. In turn, the SA will produce losses. Thus we propose a combined scheme of VCSEL with SA coupled with FSF with this anticipation that SA will create bistability of CS, while FSF will compensate to loss. Our proposed scheme is a kind of symbiotic scheme where FSF and SA try to minimize each other's disadvantages and lead to the generation of robust bistable CSs.

In the past couple of years, experimental research on CS, based on commercially available VCSEL attracted huge interest due to its application in realizing all-optical devices, it can be used as, 'bits' of information, erasable memory etc. Reports have come out on the writing and erasing [5, 20, 21], creation and annihilation [22, 23] and space-time dynamics of localized structures in cavity, particularly in VCSEL [24]. The theoretical study of CSs is not a little less important, rather attained a significant height due to its complex yet elegent mathematical formulation, intriguing dynamical behaviour and multidisciplinary characteristics. The mathematical modeling of CS generally involves complex Ginzburg-Landau equation(CGLE), complex Swift-Hohenberg equation (CSHE) or Lugiato-Lefever equation (LLE). Due to the intricacy and non-integrability, investigations on practically relevant equations are mostly driven by numerical methods and simulations. On the other hand, for the development of an insightful and comprehensive theory the necessity of analytical method is inevitable. But the problem is, only certain types of such equations are integrable and have exact soliton solutions. That is too when certain constraints are imposed on the system parameters [2]. Cole-Hopf transformation may be useful for obtaining exact solution for some nonlinear equations, e.g. Burger's equation and Koshi's problem, by reducing the nonlinear dissipative equations into linear one [25]. But real systems can be represented by so complicated nonlinear equations that such reduction is not feasible. Methods have been developed to get closed form analytical expression for solitary wave of non-integrable nonlinear systems. Among them the 'Truncation methods' are rather easier [26]. But since it a priori assumes certain forms of ansatz, other types of potential solution are overlooked. A better method involves constructing intermediate first-order autonomous ordinary differential equation and computer algebra to explore a large variety of solitary wave solutions. For more details one can go through reference [26] and the references therein. The above mentioned methods suffer from serious drawbacks owing to the tediousness of procedure and/or the complicated nature of the solution. In this context separation method, which has been successfully predicted dissipative CS for a large variety of systems, could be an efficient

rescuer [7]. Instead of obtaining the exact solution this method emphasizes in locating the stability region. It involves splitting of the governing rate equation into two Eigen-value equations; a linear or spectral problem and a nonlinear or soliton problem and solving them graphically for soliton solution. Although the method can provide 'tailor made' solutions and even predict the stability, it doesn't explicitly portrays the evolution of the soliton parameters. In this context variational method can be a good alternative. It can explicitly display the information of each soliton parameter during evolution. Also, variational method can predict the stability region in parametric space using different stability criteria such as Lyapunov criterion and Hurwitz conditions [27]. The variational approach has been used to find bistable solitary waves of first kind in D-dimension [28]. It has been applied to nonlinear dissipative pulse propagation in the presence of two- photon absorption [29]. Also dissipative solitonic pulse in multi-dimension are predicted with variational method [27]. Still this method has merely been sought for investigating CS. In the current investigation, variational method is comprehensively used for complete investigation of CS and its stability in one-, two- and three-dimensional systems.

The most amazing phenomena related to CS comes probably in the form of CS dynamics and their interaction. Any gradient, such as, phase, thermal, intensity, cavity length and inhomogeneous cavity resonance [12, 30–33] in the VCSEL causes the spontaneous drift of the CS. Sometimes the movement is rotational, like a binary star's rotation around a barycenter [34]. Even, billiards ball like movement of CS, where a CS self-propels along a closed square orbit (both clockwise and counter-clockwise) has been reported [35]. Gradient induced CS dynamics is perceptible due to the large cross-sectional area of the VCSEL device [34]. Besides the gradient induced CS drift interaction of two or more CSs are important due to two reasons. Firstly, to verify the fundamental criteria of soliton; secondly, and more importantly, for the quest of intriguing all-optical phenomena. Interaction behavior of CS is controlled by separation distances between injected CS, thermal instabilities and relative phase [36, 37]. Here, we investigate the interaction of CS with different phases, with the anticipation of phase controlled all-optical CS dynamics.

The organization of this paper is as follows. The variational method based mathematical formulation is developed in section 2. Section 3 contains the detailed analytical study of existence and stability analysis along with bifurcation analysis of the system. CSs of one-, two- and three-dimensions are obtained by variational method in section 4. The analytical results are validated by numerical analysis in the same section. Section 5 deals with the interaction of the CS in the cubic-quintic nonlinear material followed by an application-defining conclusion.

2. FEEDBACK AND SATURABLE ABSORBER MODEL: A VARIATIONAL FORMULATION

The dissipative system we consider comprises of VCSEL with SA and coupled with FSF. In the framework of mean-field cavity model, the cavity field $E(r, t)$ and feedback field $F(r, t)$ can be represented by the following dynamical equations in conjugation with the rate equations of the carrier density for active and passive materials and the feedback field [7, 8, 25, 38].

$$\frac{\partial E}{\partial t} = [-(1 - i\theta) + (1 - i\alpha)d_a + (1 - i\beta)d_p + i\Delta_\perp]E + F, \quad \textbf{(1)}$$

$$\frac{\partial d_a}{\partial t} = c_1[d_a(1 + |E|^2) - \mu], \qquad (2)$$

$$\frac{\partial d_p}{\partial t} = c_2[d_p(1 + s|E|^2) + \gamma], \qquad (3)$$

$$\frac{\partial F}{\partial t} = -(\lambda + i\Omega_0)F + \sigma\lambda E. \qquad (4)$$

Here we considered an external cavity short enough to introduce negligible delay in the system. Otherwise, presence of a significant delay may lead to chaotic behavior of the CS [39]. In view of the cylindrical geometry of VCSEL, a symmetric system of equations is best fitted. Here, r is the transverse spatial co-ordinate and t is time normalized to the cavity roundtrip period. On right hand side of equation (1), first term describes the linear losses incurred by the system. The '1' is the normalized cavity loss and θ is the mis-tuning between the frequencies of feedback field and cavity that measures the mismatch between the feedback and cavity frequencies. θ needs to be small in order to reduce linear losses. μ and α respectively represent the pump parameter and linewidth enhancement factor for active materials, while those for passive materials are given by γ and β respectively. α and β usually possess positive and large values for VCSEL. Thus, second and third terms on the right hand side of equation (1) represent carrier densities. Carrier density in active material is represented by d_a, whereas, in passive material is represented by d_p. The fourth term represents the diffraction with $\Delta_\perp = r^{(1-D)}\frac{\partial}{\partial r}(r^{(D-1)}\frac{\partial}{\partial r})$ being the transverse Laplacian, represents diffraction operator for D-dimensional system. c_1 and c_2 are the ratio of the photon lifetime to the carrier lifetime in the active and passive materials, respectively. Coupling of the linear feedback field with cavity field leads to the stabilization of the system [7]. Frequency selective feedback is provided by a DBR. In equation (4), σ represents the feedback strength that needs to be positive, so as to provide gain in the cavity. It always assumes a value between 0 and 1. The frequency selection of feedback is accomplished by a filter and λ represents the band-width of filter reflection, and resonance frequency of feedback field is represented by Ω_0. However, losses cannot be eliminated completely. At steady state the carrier density for active and passive materials, as well as feedback consider the following condition i.e., $\partial d_a/\partial t = 0$, $\partial d_p/\partial t = 0$ and $\partial F/\partial t = 0$. Equations (1), (2), (3) and (4) can be combined as:

$$\frac{\partial E}{\partial t} = [-(1 - i\theta) + \frac{\mu(1 - i\alpha)}{1 + |E|^2} - \frac{\gamma(1 - i\beta)}{1 + s|E|^2} + i\Delta_\perp]E$$
$$+ (a + ib)E, \qquad (5)$$

where, $a = \sigma\lambda^2/(\lambda^2 + \Omega_0^2)$ and $b = \sigma\lambda\Omega_0/(\lambda^2 + \Omega_0^2)$. Expanding the terms $(1 + |E|^2)^{-1}$ and $(1 + s|E|^2)^{-1}$, in equation (5), up to second order and rearranging, the following cubic-quintic CGLE (CGLE5) is obtained:

$$\frac{\partial E}{\partial t} = i\Delta_\perp E + (m_1 + im_2)E + (m_3 + im_4)|E|^2E$$
$$+ (m_5 + im_6)|E|^4E. \qquad (6)$$

Here, $m_1 = \mu - 1 - \gamma + a$, $m_2 = \theta - \alpha\mu + \beta\gamma - b$, $m_3 = s\gamma - \mu$, $m_4 = \alpha\mu + s\gamma\beta$, $m_5 = \mu - s^2\gamma$ and $m_6 = s^2\beta\gamma - \alpha\mu$.

Although, quintic nonlinearity is considerably smaller in comparison to the cubic (Kerr) one, yet the quintic terms significantly modifies system dynamics. Moreover, being a higher order nonlinearity, quintic nonlinearity plays an important role in the stability of a soliton. Although equation (6) is well studied in the context of conventional propagating soliton, it has never been used for the investigation of CS, which can be considered as a "soliton in a box", or a bound state of a propagating soliton bouncing between the cavity mirrors. While evolution of conventional soliton is described along propagation length (z) that for CS to be described with respect to time. The confinement feature and time evolution makes CS completely exclusive among spatial dissipative soliton. Equation (6) is made suitable for such a special case by replacing z by time, which is normalized to the cavity round trip time and considering all of the CS parameters as function of the normalized time instead of function of z. Now equation (6) is not only compatible with CS system but also can enjoy all the benefits of already known features of equation (6). The CGLE5 (i.e. equation 5) is non-integrable. However, exact solution can be obtained only in some particular case [40, 41]. The common approach is to solve the CGLE5 by numerical methods. But to get greater insight of the behavior of the individual parameters the necessity of the analytic approach is indispensable. Therefore, we use a complete variational method based approach to study the CGLE5. Separating into conservative and dissipative parts, equation (6) can be rewritten as:

$$i\frac{\partial E}{\partial t} + \Delta_\perp E + m_2E + m_4|E|^2E + m_6|E|^4E = Q. \qquad (7)$$

Here,

$$Q = i(m_1E + m_3|E|^2E + m_5|E|^4E), \qquad (8)$$

is the dissipative part, in absence of which equation (7) turns into a conservative Nonlinear Schrödinger equation (NLSE). The Lagrangian corresponding to the conservative part, i.e., left hand side of equation (7) is given by:

$$\mathbb{L}_C = r^{(D-1)}[\frac{i}{2}(E\frac{\partial E^*}{\partial t} - E^*\frac{\partial E}{\partial t}) + |\frac{\partial E}{\partial r}|^2 - m_2|E|^2$$
$$- \frac{m_4}{2}|E|^4 - \frac{m_6}{3}|E|^6]. \qquad (9)$$

For the dissipative part, i.e., equation 8, the Lagrangian can be constructed as:

$$\mathbb{L}_Q = ir^{(D-1)}[m_1|E|^2 + \frac{m_4}{2}|E|^4 + \frac{m_6}{3}|E|^6] \qquad (10)$$

A suitable ansatz or trial function is now required. The choice of trial function in variational method is always crucial for the success of the investigation. The exact soliton ansatz of this type of equation (7) is given by Pushkarov et al. [42] and de Anglis [43]. However, theoretically predicted and experimentally obtained CSs are mostly for bell-shaped intensity profile. Sech is the preferred profile for analytical as well as numerical modelling [7]. For the present case a Gaussian trial function of the following form, which is very close to sech profile yet easier for mathematical treatment is useful [27].

$$E(r, t) = A \exp(-\frac{r^2}{2R^2} + iCr^2 + i\phi), \qquad (11)$$

$A(t)$, $R(t)$, $C(t)$ and $\phi(t)$ are functions of t and refer to amplitude, width, chirp and phase of the profile, respectively. Notably, the parameters are presented as function of time. In case of

propagating soliton the evolution axis is propagation direction z, i.e., the evolution term is given by $\partial E/\partial z$. There the usual practice is to write the parameters as functions of space, e.g., $A(z)$, $R(z)$, $C(z)$ and $\phi(z)$. For our CGLE, time is the evolution axis, i.e., $\partial E/\partial t$ is the evolution term. Accordingly, the z dependent parameters of trial function can be replaced by t dependent ones. Substituting the aforesaid trial function in equation (9), the reduced Lagrangian for conservative part takes the form:

$$\mathbb{L}_C = r^{(D-1)}[(\frac{\partial \phi}{\partial t} - m_2)A^2 exp(-\frac{r^2}{R^2})$$
$$+(\frac{\partial C}{\partial t} + \frac{1}{R^4} + 4C^2)A^2r^2exp(-\frac{r^2}{R^2})$$
$$-\frac{m_4}{2}A^4exp(-\frac{2r^2}{R^2}) - \frac{m_6}{3}A^6exp(-\frac{3r^2}{R^2})]. \quad (12)$$

Corresponding, total Lagrangian can be determined as:

$$L_C = \int \mathbb{L}_C dr. \quad (13)$$

$$L_C = [\frac{A^2R^D}{2}(\frac{\partial \phi}{\partial t} - m_{20}) + \frac{D}{4}A^2R^{(D+2)}(\frac{\partial C}{\partial t} + \frac{1}{R^4} + 4C^2)$$
$$-\frac{m_{40}}{2}A^4R^D - \frac{m_{60}}{2}A^6R^D]\Gamma(\frac{D}{2})(1 + (-1)^{(D+1)}), \quad (14)$$

where, $\Gamma(n)$, is the gamma function. The parameters m_1, m_2, m_3, m_4, m_5 and m_6 are normalized as $m_{10} = m_1$, $m_{20} = m_2$, $m_{30} = m_3 2^{(-\frac{D}{2}-1)}$, $m_{40} = m_4 2^{(-\frac{D}{2}-1)}$, $m_{50} = m_5 3^{(-\frac{D}{2}-1)}$ and $m_{60} = m_6 3^{(-\frac{D}{2}-1)}$. The Euler-Lagrangian equation for dissipative system is defined as [27]:

$$\frac{\partial}{\partial t}(\frac{\partial L_C}{\partial \eta\prime}) - \frac{\partial L_C}{\partial \eta} = 2Re \int r^{(D-1)}Q\frac{\partial E^*}{\partial \eta}dr. \quad (15)$$

where, η can be any of the soliton parameters, i.e., $\eta(t) = A(t)$, $R(t)$, $C(t)$ and $\phi(t)$, $\eta\prime = \partial\eta/\partial t$ and E^* is the complex conjugate of E. The variations of Lagrangian with respect to the amplitude $A(t)$, inverse width $R(t)$, chirp $C(t)$ and phase $\phi(t)$ yield the following set of equations:

$$(\frac{\partial \phi}{\partial t} - m_{20}) + \frac{D}{2}R^2(\frac{\partial C}{\partial t} + \frac{1}{R^4} + 4C^2) - 2m_{40}A^2 - 3m_{60}A^4 = 0,$$
$$\quad (16)$$

$$(\frac{\partial \phi}{\partial t} - m_{20}) + (\frac{D}{2} + 1)R^2(\frac{\partial C}{\partial t} + \frac{1}{R^4} + 4C^2) - \frac{2}{R^2}$$
$$-m_{40}A^2 - m_{60}A^4 = 0, \quad (17)$$

$$\frac{\partial}{\partial t}(A^2R^{(D+2)}) - 8A^2CR^{D+2} = 2m_{10}A^2R^{D+2}$$
$$+2m_{30}A^4R^{D+2} + 2m_{50}A^6R^{(D+2)}, \quad (18)$$

and

$$\frac{\partial}{\partial t}(A^2R^D) = 2m_{10}A^2R^D + 2m_{30}A^4R^D + 6m_{50}A^6R^D. \quad (19)$$

Equations (18) and (19) show that the power $(P = A^2R^D)$ is not a constant quantity with respect to time, which is usually a constant for conservative systems. Solving equations (16), (17), (18) and (19) the evolution equations of A, R, C and ϕ are obtained as follows:

$$T_1 = \frac{\partial A}{\partial t} = 2DAC - m_{10}A - (\frac{D}{2} + 2)m_{30}A^3$$
$$-(D+3)m_{50}A^5, \quad (20)$$

$$T_2 = \frac{\partial R}{\partial t} = 4CR - m_{30}A^2R - 2m_{50}A^4R, \quad (21)$$

$$T_3 = \frac{\partial C}{\partial t} = \frac{1}{R^4} - 4C^2 - m_{40}\frac{A^2}{R^2} - 2m_{60}\frac{A^4}{R^2}, \quad (22)$$

and

$$\frac{\partial \phi}{\partial t} = m_{20} - \frac{D}{R^2} + (\frac{D}{2} + 2)m_{40}A^2 + (D+3)m_{60}A^4. \quad (23)$$

3. STABILITY ANALYSIS

Like other dissipative solitons, CS formulation involves confluence of three major concepts, namely, the standard concept of soliton theory, the theory of nonlinear dynamics and the concept of a system far from an equilibrium [25]. The stability analysis of the system is therefore inevitable for knowing the system sustainability. Equations (20), (21) and (22) can be employed to analyze the system stability. The steady state solution of amplitude for the dissipative system, can attain two possible values given as:

$$A_\pm = \sqrt{\frac{-m_{30} \pm \sqrt{m_{30}^2 - 3m_{50}m_{10}}}{3m_{50}}}. \quad (24)$$

The steady state solutions for CS chirp and width are given by following equations respectively:

$$C = \frac{m_{30}}{4}A^2 + \frac{m_{50}}{2}A^4, \quad (25)$$

$$R_\pm = \sqrt{\frac{-(m_{40}A^2 + 2m_{60}A^4) \pm \sqrt{(m_{40}A^2 + 2m_{60}A^4)^2 + 16C^2}}{8C^2}}. \quad (26)$$

To establish stability criteria, Lyapunov stability analysis is employed to the system. Evolution equations (20), (21), (22) and (23) obtained by the Variational treatment of the CGLE are the ingredient to determine the stability criteria. The Jacobi determinant for the set of equations (20), (21) and (22) can be written as: $|J - \lambda I| = 0$.

$$\begin{vmatrix} \frac{\partial T_1}{\partial A} - \lambda & \frac{\partial T_1}{\partial R} & \frac{\partial T_1}{\partial C} \\ \frac{\partial T_2}{\partial A} & \frac{\partial T_2}{\partial R} - \lambda & \frac{\partial T_2}{\partial C} \\ \frac{\partial T_3}{\partial A} & \frac{\partial T_3}{\partial R} & \frac{\partial T_3}{\partial C} - \lambda \end{vmatrix}_{eq} = 0. \quad (27)$$

The corresponding characteristic Eigen value equation is given by:

$$\lambda^3 + \alpha_1\lambda^2 + \alpha_2\lambda + \alpha_3 = 0. \quad (28)$$

The coefficients of equation (28) can be determined as:

$$\alpha_1 = 2(2-D)C + m_{10} + (\frac{3D}{2} + 5)m_{30}A^2 + (5D + 17)m_{50}A^4, \quad (29)$$

$$\alpha_2 = -8(D+4)C + 4(D+8)m_{30}A^2C + (12D + 76)m_{50}A^4C + \frac{16}{R^4}$$
$$+(4C + m_{30} + 2m_{50}A^2)m_{10}A^2 + 3(\frac{D}{2} + 2)m_{30}^2A^2 + 10(D+3)m_{50}^2A^8$$
$$+(8D + 27)m_{30}m_{50}A^6 + 4(D-2)m_{40}\frac{A^2}{R^2} + 16(D-1)m_{60}\frac{A^4}{R^2}, \quad (30)$$

$$\alpha_3 = (2m_{10} - 4DC + (D+12)A^2 + 10(D+3)m_{50}A^4)\frac{8}{R^4}$$

$$-16(m_{60}(2DC + m_{10}) + 3m_{30}m_{40})\frac{A^4}{R^2} + 8((D-12)m_{30}m_{60}A^2$$

$$-6m_{30}m_{40} - 15m_{40}m_{50}A^2 - 2(D+15)m_{50}m_{60}A^4)\frac{A^4}{R^2} + 64DC^3$$

$$-((64D + 198)m_{30} + 32m_{10} + 32m_{50}DA^3R + 160(D+3)m_{50}A^4)C^2$$

$$+8m_{50}(10(D+3)m_{50}A^2 + 3(D+4)m_{30})A^5RC$$

$$+8m_{50}(5(D+3)m_{30}A^2C - 8DR^4)A^4, \quad (31)$$

The steady state of dynamical system is stable only if the real part of the roots of cubic Eigen value equation are positive. In order to establish Lyapunov stability, Hurwitz's conditions must be satisfied, i.e. all αs need to attain positive real value. Hurwitz principal minors are given by:

$$\alpha_4 = \alpha_1\alpha_2 - \alpha_3, \quad (32)$$

and

$$\alpha_5 = -(\alpha_1)^2(\alpha_2)^2 + 4(\alpha_2)^3 + 4(\alpha_1)^3\alpha_3 - 18\alpha_1\alpha_2\alpha_3 + 27(\alpha_3)^3. \quad (33)$$

To satisfy the Hurwitz conditions alike α_1, α_2 and α_3, the value of α_4 too needs to be positive. The coefficient α_5 classifies the nature of dynamical behavior of the system. The positive valued real part of α_5 indicates the stable focus whereas the negative value indicates stable node. To identify the stability region we draw contour plots of all αs in the same window with σ and μ as independent variables. Figures 1, 2 and 3 present such contour and hence stability plot, for dimensions $D = 1$, 2 and 3 respectively. In each figure curves 'a', 'b', 'c' and 'e' represent the contours of α_1, α_3, α_4 and α_2 respectively. Curves 'd' represent the discriminant of steady state quadratic equation in A^2. In each figure (figures 1, 2 and 3) the shaded region corresponds to positive values of all αs, thus represent the stable region. Any point in the stability region can give rise to a stable CS. Notably, the area of the stability region drastically shrinks in higher dimensions. The simple logic behind this is the fact that stabilizing a soliton of higher dimension is tougher.
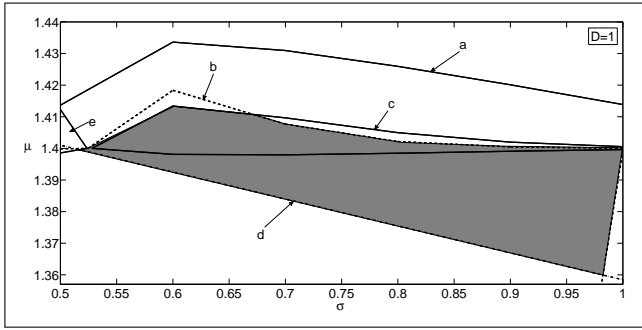
Fig. 1. Stability region corresponding to D=1. Here, $\theta = 1.2$, $\alpha = 2.7$, $\beta = 1$, $\lambda = 0.03$, $\gamma = 0.5$, $s = 10$ and $\Omega_0 = 0.1$.

Having located the parametric stability region, we will now study the influence of the system parameters on the global behavior of the system and search for bifurcation, if any. In nonlinear dynamics, bifurcation or any transition points of solutions are always the subject of ample interest. The nature of the transition points and any qualitative change therein decides the system behavior. Figures 4, 5 and 6 represent the variation of steady state A, R and C with respect to feedback strength σ for D=1, 2 and 3, respectively. The steady state value of A given by equation
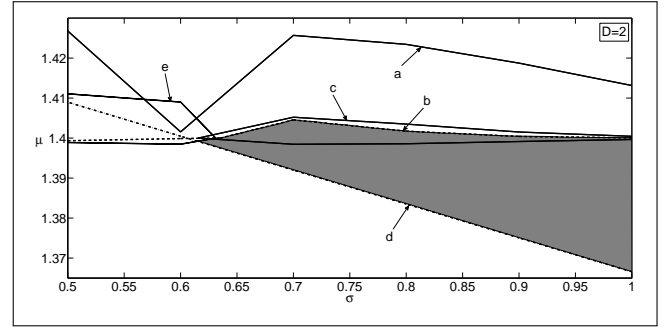
Fig. 2. Stability region corresponding to D=2. Other parameters are the same as stated in figure 1.
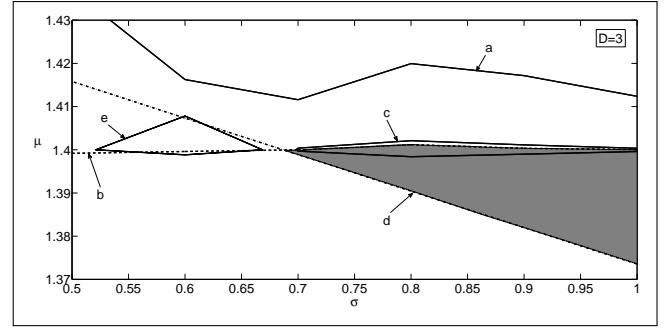
Fig. 3. Stability region corresponding to D=3. Parameter used are same as stated in figure 1.

(24), bifurcates at a particular value of $\sigma(= 0.610)$, gives rise to a stable branch (solid line, A_+) and an unstable branch (dashed line, A_-) in figure 4(a). For both the branches stability has been thoroughly checked by analytical as well as numerical methods. Similar to figure 4(a), figure 4(b) shows the bifurcation of R at same σ value, however, R_+ and R_- intersects once thereafter. Analysis revels that R_+ corresponds to stable branch, while R_- yields unstable CS. Figure 4(c) shows the bifurcation of steady state C. C_+ and C_- stand for the steady state value of C (given by equation 25) corresponding to A_+ and A_- respectively. In this case C_+ and C_- emerge as stable and unstable branches, respectively. In order to check the bifurcation behavior in higher dimension, we plotted similar bifurcation diagrams for D=2 in figure 5 and D=3 in figure 6. It is observed that as the dimension of the system increases, the bifurcation occurs at higher σ-value ($\sigma = 0.702$ for $D = 2$ and $\sigma = 0.783$ for $D = 3$), i.e., at stronger feedback. Not only the CS, the background ($E = 0$) should be stable for sustained CS. Generally, cavity parameters decide the stability of background. In this case for a stable background, m_1 (which is a function of pump parameters for active and passive materials, feedback strength, bandwidth of filter reflection and resonance frequency) should be negative.

At this point it is in order to discuss how different the CS obtained with our combined model (i.e., FSF+SA) from those obtained either with FSF or SA. The presence of SA in our model expands the CS stability zone significantly. Figure 7c portrays the spreading of CS stability zone with increasing strength of SA for $D = 1$. This wider parametric zone provides greater freedom to set input values in experimental setup that eventually eases the search of CS manifold. The bifurcation diagrams in figures 4, 5 and 6 indicate the bistable behavior of CS. Removal of SA terms from equation (5) immediately ceases the
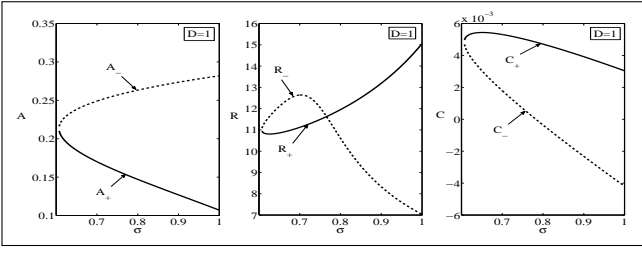
Fig. 4. Bifurcation of steady state value of (a) A, (b) R and (c) C with respect to σ for $D = 1$. Solid lines represent the stable solutions and dashed lines represent unstable solutions.
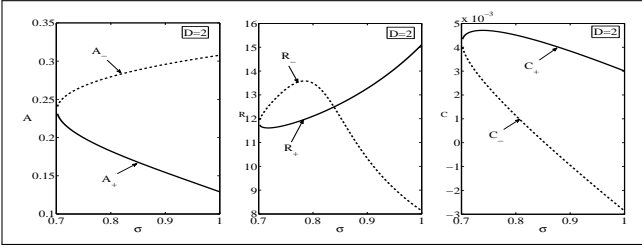
Fig. 5. Bifurcation of steady state value of (a) A, (b) R and (c) C with respect to σ for D=2. Solid lines represent the stable solutions and dashed lines represent unstable solutions.
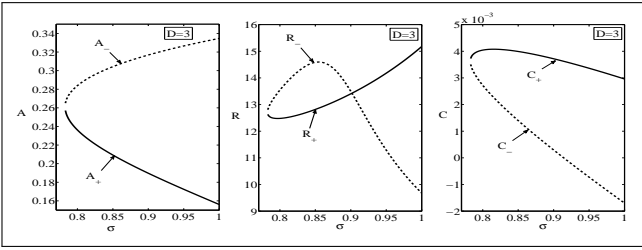
Fig. 6. Bifurcation of steady state value of (a) A, (b) R and (c) C with respect to σ for D=3. Solid lines represent the stable solutions and dashed lines represent unstable solutions.

bifurcation nature of the system. This confirms that SA is responsible for bistability. This is further supported by Figure 8, wherein the bistable CS exist in the range $\mu_{tp} < \mu < \mu_{th}$. Here, $\mu_{th} = 1 + \gamma - a$, measures the pump parameter corresponding to laser threshold for which bistability is observed and $\mu_{tp} = (\sqrt{(1-a)(s-1)} + \sqrt{\gamma})^2/s$ determines the pump parameter value at the turning point of the C-shaped bistability curve. The stability criterion is found to be $s > 1 + (1-a)/\gamma$. In this case too, the bistability of CS immediately ceases in absence of SA. Further, both μ_{th} ($= 1.4395$) and μ_{tp} ($= 1.3068$) corresponding to the combined scheme is smaller than those without FSF (1.5 and 1.3743, respectively). That means with our combined scheme the bistable CS can be generated at lower pump parameter. More importantly, the bistability range ($\delta\mu = \mu_{th} - \mu_{tp}$) of CS is significantly large ($= 0.1327$) for the combined scheme in comparison to the scheme without FSF (i.e., $= 0.1257$). Thus our combined scheme of FSF and SA in one hand spawns bistability of CS, in the other hand enlarges the CS stability range and lowers the requirement of pump energy for CS generation. All these factors may make our model preferable for experiments and applications.
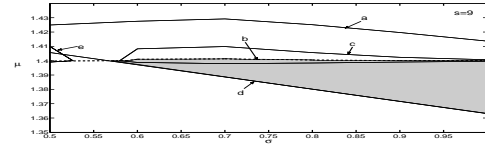
(a)
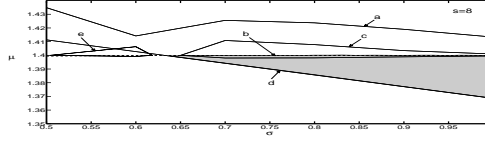
(b)
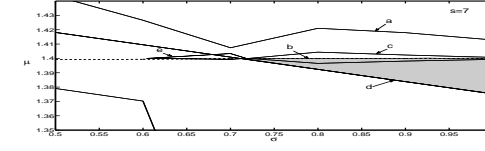
(c)

Fig. 7. Expansion of stability region with increase in saturation parameter for $D = 1$. (a), (b) and (c), respectively, correspond to the saturation parameter $s = 7, 8$ and 9.
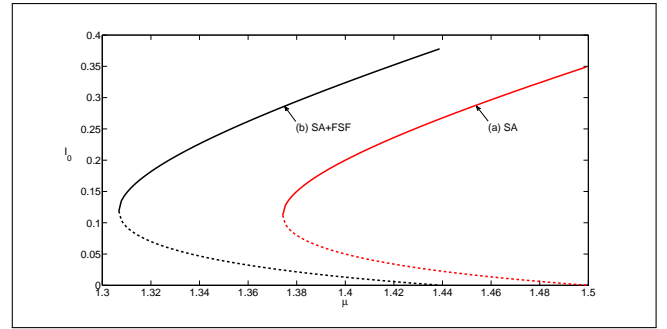
Fig. 8. Variation of field intensity of CS with pump parameter μ for the schemes with SA (curve a) and combined (SA+FSF) (curve b). The 'C' like curves show bistablity of CS. Upper branches of both the curves correspond to stable CS, while the dotted lower curve correspond to unstable CS solution.

4. EXCITATION OF ONE-, TWO- AND THREE-DIMENSIONAL CAVITY SOLITONS

With the knowledge of parametric stability region and bifurcation behavior of the soliton parameters, we now proceed to find the evolution of A_+, R_+ and C. Henceforth, for brevity we will write A_+, R_+ and C_+ as A, R and C respectively. The variationally obtained evolution equations are now solved taking points from stability region and setting points of stable branch of bifurcation diagram as initial conditions. Figures 9 represents the time evolution of A, R, C and ϕ in $D = 1$, while figures 10 and 11 portray the same for D=2 and 3 respectively. Evolution of phase ϕ can be obtained from the equation (23) with the steady state value of A, R and C obtained by equations (20), (21) and (22). For all three dimensions, A, R, C and ϕ show steady state evolution. A magnified view (in the insets of figures 9, 10 and 11) reveals some tiny initial fluctuations that quickly settle in periodic oscillations of very small amplitudes. All these confined minor oscillations suggests, the evolution of stable CS. The

evolution pattern is checked extensively for numerous points in the stability regions of all three dimensions and similar stable evolution of soliton parameters are obtained. Phase diagrams for $D = 1$, 2 and 3, drawn in figure 12 (a), (c) and (e), respectively, show the confinement of A and R. The system of smaller dimension is less prone to fluctuations as compared to that of higher dimensional system. Figure 12 (b), (d) and (f) depicts that power for a dissipative system is not constant, rather it is oscillating but confined as the system evolves with time. The steady time-evolution of soliton parameters and confined phase diagrams indicate the generation and robustness of the stable CS in all three dimensions.
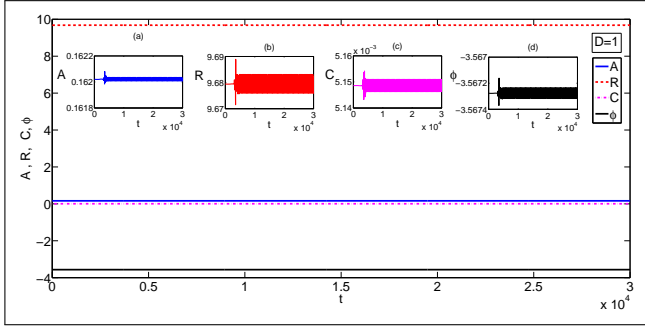
Fig. 9. The steady state evolution of A, R, C and ϕ in D=1. $\sigma = 0.7323$, $\mu = 1.3919$ and rest of the parameters as stated in figure 1. Insets show the zoom in view of the time-evolution of parameters (a) A, (b) R, (c) C and (d) ϕ.
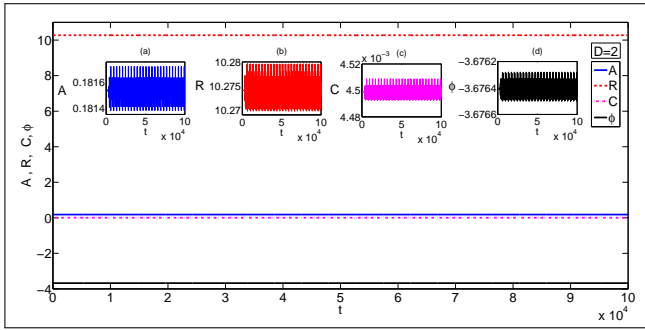
Fig. 10. The steady state evolution of A, R, C and ϕ in D=2. $\sigma = 0.8023$ and other parameter are same as stated in figure 9. Insets show the zoom in view of the time-evolution of parameters (a) A, (b) R, (c) C and (d) ϕ.

In order to validate the variationally obtained result, direct numerical solution of equation 6 is in order. Crank-Nicolson [27], Split-step Fourier method (SSFM) [13] and Runge-Kutta method are commonly used numerical methods for solving CGLE. For the present investigation SSFM is adopted to find CS corresponding to the points in the analytically obtained stability region. To our utter satisfaction, almost all the points corresponding to the stability region yield CS numerically. A typical numerically obtained CS is portrayed through several snapshots in figure 13. Thus our variational result is successful in predicting CS efficiently. In a further attempt to find the snaking [1], a typical bistable behavior of pattern forming or CS host system, the steady state values of A and R (in $D = 1$) are calculated for a range of bifurcation parameter σ. A versus R plot shows snaking in figure 14. However, one may not expect 'many stairs' in
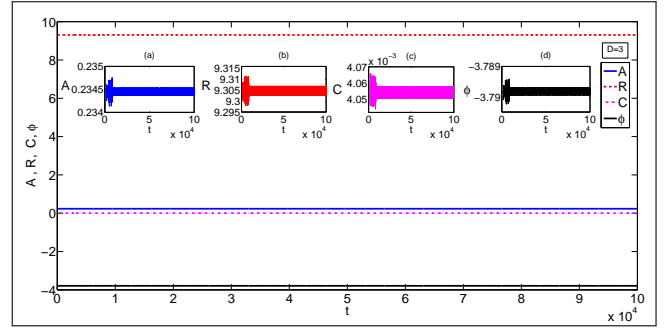
Fig. 11. The steady state evolution of A, R, C and ϕ in D=3. Parameter used are same as stated in figure 10. Insets show the zoom in view of the time-evolution of parameters (a) A, (b) R, (c) C and (d) ϕ.
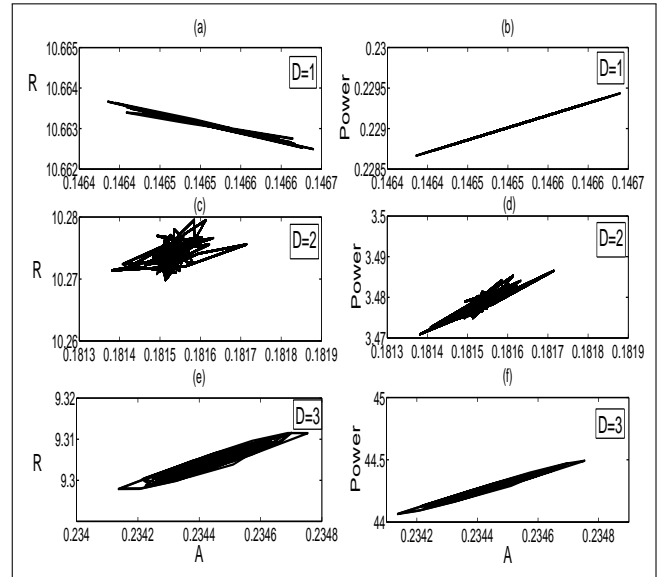
Fig. 12. Phase plots (A versus R) for (a) $D = 1$, (c) $D = 2$ and (e) $D = 3$. Amplitude of oscillation increases with dimension but remains confined. Power versus A during evolution for (b) $D = 1$, (d) $D = 2$ and (f) $D = 3$.

the snaking diagram through variational results. Points on the dashed line, which resembles with snaking curve, yield stable CS following analytical method. However, numerically, stable CS is found for the particular range of bifurcation parameter $\sigma = 0.6320$ to 0.7550. For σ-values near 0.7550 initially a breather-like soliton behavior is observed, that quickly, i.e., after few hundreds of initial steps, converts to the stable CS (Figure 15). Below $\sigma = 0.7500$ the initial turbulence almost disappears and stable CS is observed. Figure 16 shows a typical CS in that range of σ in spatio-temporal domain. Corresponding phase portrait, given in figure 17, clearly indicates the localization of CS.

5. INTERACTION

To have a complete idea about any soliton and hence CS, the study of interaction phenomenon is indispensable. Interaction phenomenon is greatly influenced by the relative phase of the co-propagating or counter-propagating CSs as well as their individual field profiles. Also, the seperation between CSs play a vital
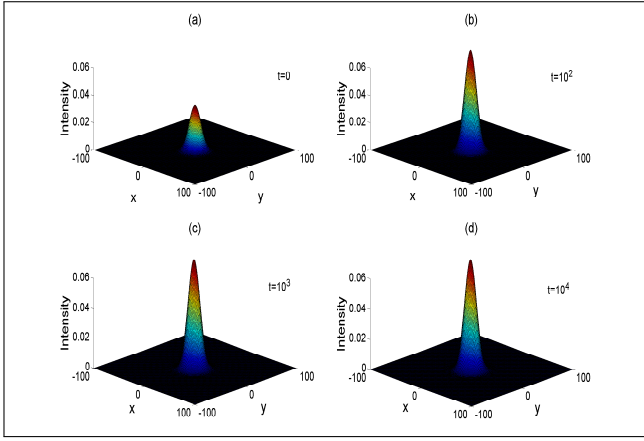
Fig. 13. Numerically obtained CS in $D = 2$ at different time of evolution. System parameters and initial values of soliton parameters are in accordance with the stability region of figure 2 and stable branches of figure 5.
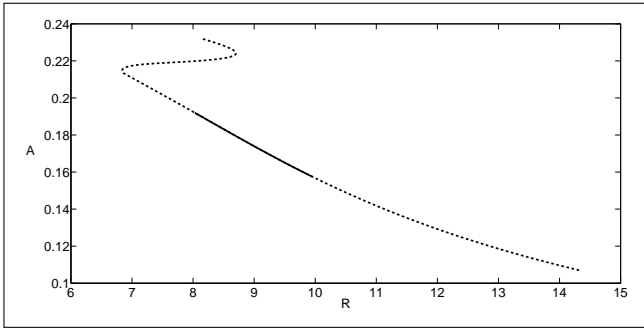
Fig. 14. Variation in steady state values of A and R with respect to the bifurcation parameter σ ($0 < \sigma < 1$) for dimensions $D = 1$. Dashed line corresponds to the analytically predicted stable CS, whereas solid line (overlaps with dashed line segment) corresponds to the numerically obtained CS. Numerically stable CS occurs for the set of A and R that corresponds to $\sigma = 0.6320$ to 0.7550.
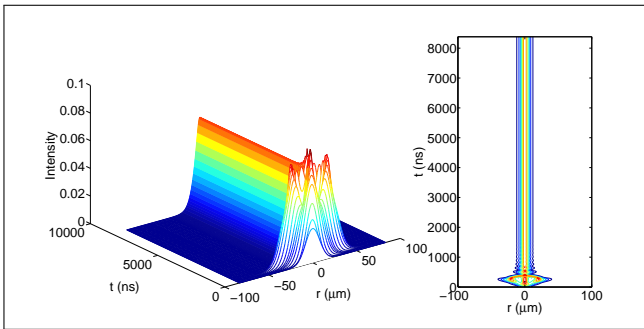
Fig. 15. Evolution of CS obtained by numerical method for $D = 1$. Initially, a breather like profile is observed, later on it regains solitonic shape and evolves undistorted. Here, $\sigma = 0.7542$, rest of the parameters are same as those used in 9 with step size $h = 0.01$. (a) spatio-temporal intensity plot and (b) shows the contour plot of the evolving profile.

role in the dynamics of interacting solitons or CS. The present investigation corresponds to the interaction between two coherent
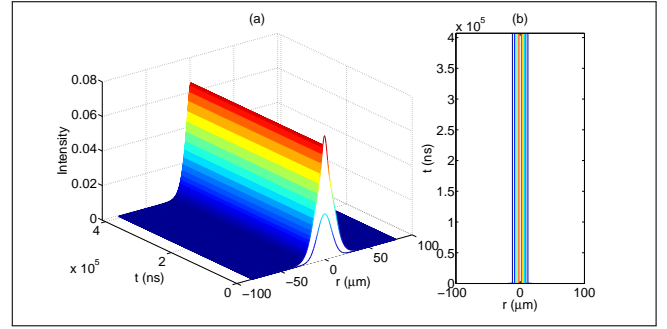
Fig. 16. Evolution of CS obtained by numerical method, for $\sigma = 0.7323$, $D = 1$ and rest of the parameters as same as those in figure 9. Step-size $h = 0.01$. (a) the spatio-temporal intensity plot and (b) the contour plot of the evolving profile. After initial turbulence, the amplitude increases and then get fixed to a steady amplitude.
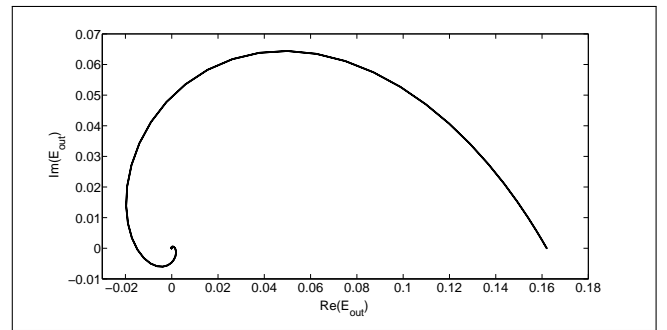
Fig. 17. The phase diagram (real versus imaginary part of the amplitude) of the output CS corresponding to figure 16.

co-propagating CSs at different relative phases. Gradient in the cavity can be introduced in terms of intensity, phase, amplitude, temperature, cavity resonance and cavity length [11, 21, 30]. Spatial drift of CS in the cavity can be influenced by any of the above stated gradients and the CS comes to rest when the gradient vanishes or CS reaches at an equilibrium state [30]. In the present investigation, the drift experienced by coupled CSs is due to the phase difference introduced between the co-propagating CSs. It has been observed that, if the initial separation between the two interacting CSs is less than two CS widths and the relative phase is zero, then fusion of the interacting CS occurs. Similar fusion occurs for a relative phase less than $\pi/2$. For a relative phase of $\pi/2$ one CS remains stationary while the other starts moving, collide with the former one to annihilate it and eventually bounces back. The soliton interaction is to be inelastic as the system is non-integrable. Separation of more than two CS widths results in no interaction between the incident CSs . Therefore, in the present investigation the initial separation of two soliton widths in-between the incident CSs is maintained and the interaction is studied at different relative phases (Figure 18). In-phase co-propagating CSs experience catastrophic collapse after propagating for about 1400 time-steps (i.e., cavity round trip time) (Figure 18a). Co-propagating in-phase CSs drift toward each other, as a result of attraction, and at a point their intensity profile overlaps and hence intensity profile shoots up, leading to the instantaneous self-focusing. Abrupt increase of the self-focusing imbalances the delicate balance with the diffraction, leading to the instability of the CS and thus resulting to the catastrophic

collapse of the system. As phase difference is increased between the two co-propagating CSs, the phase gradient is introduced in the system, causing the spatial drift of both the CSs. Figures 18b, 18c, 18d,18e and 18f represent the spatial drift of CSs for different relative phases, namely, $\pi/10$, $\pi/8$, $\pi/4$, $\pi/3$ and $\pi/2$, respectively. Due to the presence of quintic nonlinearity the CS dynamics in this case is much more intriguing than the case of a Kerr cavity. In general, the partially out-of-phase CSs (figures 18b-18f) show several attraction-repulsion cycles and eventually one gets annihilated, while the other moves with a uniform speed thereafter. The speed of the survived CS decreases nonlinearly with the increase in relative phase (figure 19). For the sake of symmetry, central point of the spatial axis is marked as zero, left CS (LCS) represents the CS formed on the negative spatial axis, whereas right CS (RCS) corresponds to the CS formed on the positive spatial axis. Also, increasing relative phase delays the annihilation of the CS. As the relative phase crosses a value of $\pi/2$, the CS velocity decreases significantly, while preserving the nature of its dynamics. For completely out-of-phase situation, CS velocity is very less but increases with the evolution. As relative phase crosses the value of π, the CS pair starts drifting in opposite direction with the increasing velocity.

(a)   **(b)**

(c)   **(d)**

(e)   **(f)**
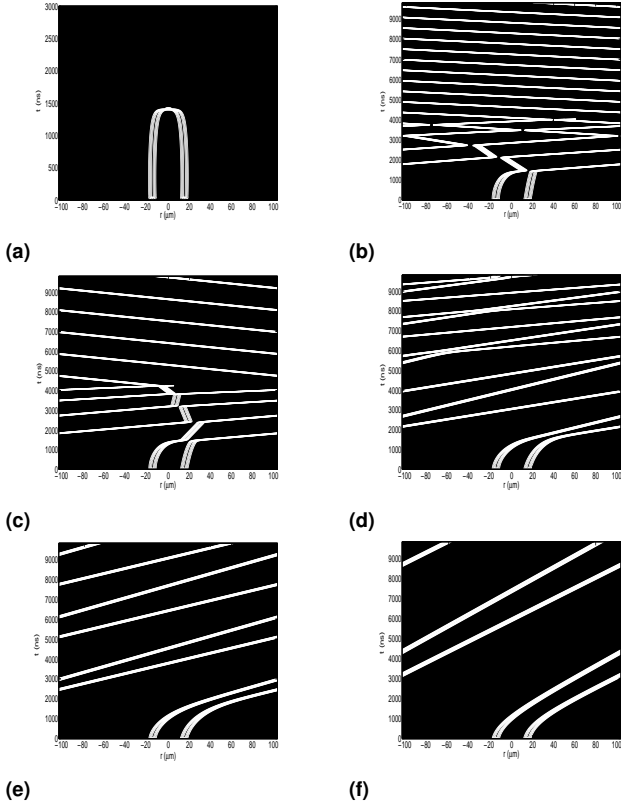
Fig. 18. Interaction of two CS at the following relative phases ($\Delta\phi$): (a) for $\Delta\phi = 0$ interacting CS experiences Catastrophic collapse, (b) and (c) for $\Delta\phi = \pi/10$ and $\Delta\phi = \pi/8$ one soliton annihilates whereas another travels with almost constant velocity, (d) for $\Delta\phi = \pi/4$ each soliton moves with changing velocity during evolution, (e) for $\Delta\phi = \pi/3$ evolution of solitons with approximately constant velocity and (f) for $\Delta\phi = \pi/2$ evolution of solitons with slightly different velocities.

More insight can be obtained by precisely looking on the velocities of an individual CS. Considering figure 18d, wherein
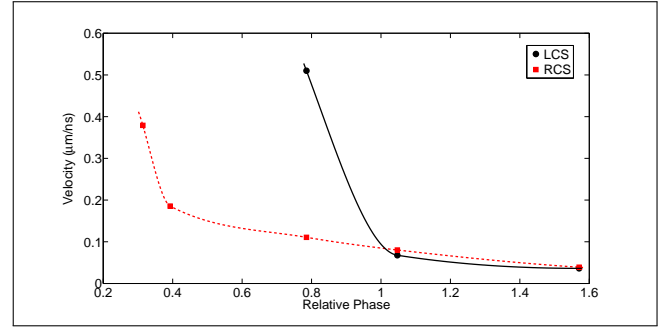
Fig. 19. Relative phase versus velocity plot for interacting CSs. Solid line represents the velocity of LCS where as dashed line corresponds to the RCS. For phase difference = $\pi/4$, the velocity is changing with time, therefore, corresponding average velocity is considered.

the velocities of both CSs change with time. The variation of CS velocities are represented in the figure 20. RCS starts with almost uniform velocity, whereas, the LCS starts with an acceleration. As LCS approaches RCS, the transfer of momentum is experienced by RCS, resulting in the increase of its velocity. On the other hand, LCS retards. Again the accelerated RCS approaches the retarded LCS. The transfer of momentum from the RCS to LCS is observed. LCS gains momentum, therefore starts moving with high velocity and RCS retards. Eventually, the LCS accelerates during the retardation phase of the RCS and vice-versa. The cycle of acceleration and retardation of LCS and RCS is repeated several times (see supplementary media). Figure 20 depicts one cycle of it. Two completely out-of-phase co-propagating CSs repel and attract each other periodically (Figure 21). The frequency of oscillation as well as the velocity of the interacting CSs increase with evolution, keeping the motion confined. The relative phase of the two interacting CSs also get modulated with evolution (figure 21b). The CSs are initially locked in out-of-phase mode, gradually move out of this locking. Besides phase, the motion of CS can be controlled by other cavity parameters, like feedback strength, delay in the feedback and even detuning. With stronger feedback strength, the velocity increases which is being reported in forthcoming communications.
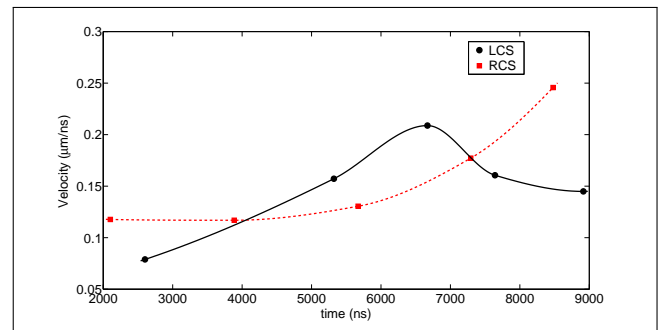
Fig. 20. Variation of the velocity of LCS and RCS with evolution for the relative phase $\pi/4$. Solid line represents the velocity of LCS where as dashed line corresponds to the RCS.
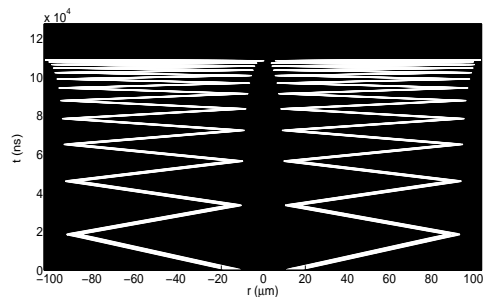
(a)
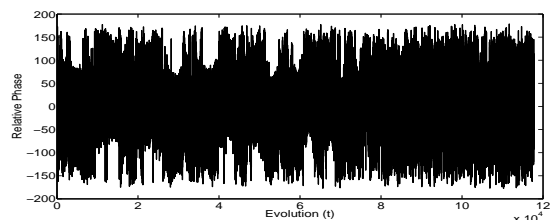
(b)

Fig. 21. (a) Space-time evolution of out-of-phase CSs. (b) Relative phase of the CSs originating in positive and negative spatial domains.

Fig. 22. This visualization shows the continuous cycle of retardation and acceleration during the evolution of interacting CS having relative phase $\pi/4$.

6. CONCLUSION

Variational method based analytical study predicts one-, two- and three-dimensional stable CS in a broad area semiconductor laser cavity comprises of vertical-cavity surface emitting laser with a saturable absorber and coupled to a frequency-selective feedback element. Analytical solution of the system defining complex Ginzburg-Landau equation in conjugation with Lyapunov stability analysis locates the region of stable CS. The higher the dimension the smaller the stability region. Bifurcation diagram are drawn to show stable and unstable branches of cavity soliton parameters. Analytically determined CS are verified by direct numerical solution of the governing equation using split-step Fourier method. Localization of CS is achieved for one, two and three dimensions. Also, snaking behavior of the system is shown. The interaction of two CSs demonstrate that the speed of the CSs can be controlled by their relative phase. Even the CS can be annihilated by controlling the phase. CS thus achieved are suitable 'bits' for information, hence can be used for data storage and processing, imaging and related all-optical devices that can be used in optical information technology.

7. SUPPLEMENTAL MATERIAL

This section presents the supplementary visualization of the interaction corresponding to the relative phase $\pi/4$ (media file 22).

8. FUNDING INFORMATION

REFERENCES

1. T. Ackemann, W. J. Firth, and G.-L. Oppo, "Fundamentals and applications of spatial dissipative solitons in photonic devices," in "Advances in Atomic Molecular and Optical Physics," E. Arimondo, P. R. Berman, and C. C. Lin, eds. (Academic Press, 2009), Advances In Atomic, Molecular, and Optical Physics.
2. N. Akhmediev and A. Ankiewicz, *Solitons* (Springer US, 1997).
3. N. N. Akhmediev, A. Ankiewicz, and J. M. Soto-Crespo, "Multisoliton solutions of the complex ginzburg-landau equation," Phys. Rev. Lett. **79**, 4047–4051 (1997).
4. P. V. Paulau, A. J. Scroggie, A. Naumenko, T. Ackemann, N. A. Loiko, and W. J. Firth, "Localized traveling waves in vertical-cavity surface-emitting lasers with frequency-selective optical feedback," Phys. Rev. E **75**, 056208 (2007).
5. N. Radwell and T. Ackemann, "Characteristics of laser cavity solitons in a vertical-cavity surface-emitting laser with feedback from a volume bragg grating," IEEE J. of Quant. Electron. **45**, 1388–1395 (2009).
6. N. Akhmediev, "General theory of solitons," in "Soliton-Driven Photonics," A. D. Boardman and A. P. Sukhorukov, eds. (Springer Netherlands, 2001), NATO Science Series II.
7. W. J. Firth and P. V. Paulau, "Soliton lasers stabilized by coupling to a resonant linear system," Eur. Phys. J. D **59**, 13–21 (2010).
8. M. Bache, F. Prati, G. Tissoni, R. Kheradmand, L. Lugiato, I. Protsenko, and M. Brambilla, "Cavity soliton laser based on vcsel with saturable absorber," Appl. Phys. B **81**, 913–920 (2005).
9. X. Hachair, F. Pedaci, E. Caboche, S. Barland, M. Giudici, J. Tredicce, F. Prati, G. Tissoni, R. Kheradmand, L. Lugiato, I. Protsenko, and M. Brambilla, "Cavity solitons in a driven vcsel above threshold," IEEE J. of Sel. Top. in Quant. Electron. **12**, 339–351 (2006).
10. A. J. Scroggie, W. J. Firth, and G.-L. Oppo, "Cavity-soliton laser with frequency-selective feedback," Phys. Rev. A **80**, 013829 (2009).
11. P. V. Paulau, D. Gomila, P. Colet, M. A. Matías, N. A. Loiko, and W. J. Firth, "Drifting instabilities of cavity solitons in vertical-cavity surface-emitting lasers with frequency-selective feedback," Phys. Rev. A **80**, 023808 (2009).
12. Y. Tanguy, N. Radwell, T. Ackemann, and R. Jäger, "Characteristics of cavity solitons and drifting excitations in broad-area vertical-cavity surface-emitting lasers with frequency-selective feedback," Phys. Rev. A **78**, 023810 (2008).
13. G. P. Agrawal, *Nonlinear Fiber Optics* (Academic Press, San Diego, California, USA, 2001), 3rd ed.
14. C. Zhan, D. Zhang, D. Zhu, D. Wang, Y. Li, D. Li, Z. Lu, L. Zhao, and Y. Nie, "Third- and fifth-order optical nonlinearities in a new stilbazolium derivative," J. Opt. Soc. Am. B **19**, 369–375 (2002).
15. J. A. Goldstone and E. Garmire, "Intrinsic optical bistability in nonlinear media," Phys. Rev. Lett. **53**, 910–913 (1984).
16. N. N. Rosanov and S. V. Fedorov, "Diffraction switching waves and autosolitons in a saturable-absorber laser," Opt. Spectrosc. **72**, 1394 (1992).
17. A. Vladimirov, S. Fedorov, N. Kaliteevski, G. Khodova, and N. Rosanov, "Numerical investigation of laser localized structures," J. Opt. B: Quant. Semiclass. Opt. **1**, 101 (1999).
18. A. G. Vladimirov, G. V. Khodova, and N. N. Rosanov, "Stable bound states of one-dimensional autosolitons in a bistable laser," Phys. Rev. E **63**, 056607 (2001).
19. N. Rosanov, "Solitons in laser systems with saturable absorption," in "Dissipative Solitons," , vol. 661 of *Lecture Notes in Physics* N. Akhmediev and A. Ankiewicz, eds. (2005).
20. J. K. Jang, M. Erkintalo, S. G. Murdoch, and S. Coen, "Writing and erasing of temporal cavity solitons by direct phase modulation of the cavity driving field," Opt. Lett. **40**, 4755–4758 (2015).
21. S. Barland, J. R. Tredicce, M. Brambilla, L. A. Lugiato, S. Balle, M. Giudici, T. Maggipinto, L. Spinelli, G. Tissoni, T. Knodl, M. Miller, and

R. Jager, "Cavity solitons as pixels in semiconductor microcavities," Nature **419**, 699–702 (2002).

22. K. Luo, J. K. Jang, S. Coen, S. G. Murdoch, and M. Erkintalo, "Spontaneous creation and annihilation of temporal cavity solitons in a coherently driven passive fiber resonator," Opt. Lett. **40**, 3735–3738 (2015).

23. U. Peschel, D. Michaelis, C. Etrich, and F. Lederer, "Formation, motion, and decay of vectorial cavity solitons," Phys. Rev. E **58**, R2745–R2748 (1998).

24. M. Tlidi, E. Averlant, A. Vladimirov, A. Pimenov, S. Gurevich, and K. Panayotov, in "Structural Nonlinear Dynamics and Diagnosis," , vol. 168 of *Springer Proceedings in Physics* M. Belhaq, ed. (2015).

25. N. Akhmediev and A. Ankiewicz, "Dissipative solitons in the complex ginzburglandau and swifthohenberg equations," in "Dissipative Solitons," , vol. 661 of *Lecture Notes in Physics* N. Akhmediev and A. Ankiewicz, eds. (Springer-Verlag Berlin Heidelberg, 2005), chap. 1.

26. R. Conte and M. Musette, "Solitary waves of nonlinear non-integrable equations," in "Dissipative Solitons," , vol. 661 of *Lecture Notes in Physics* N. Akhmediev and A. Ankiewicz, eds. (2005).

27. V. Skarka and N. B. Aleksic, "Stability criterion for dissipative soliton solutions of the one-, two-, and three-dimensional complex cubic-quintic ginzburg-landau equations," Phys. Rev. Lett. **96**, 013903 (2006).

28. R. H. Enns and S. S. Rangnekar, "Variational approach to bistable solitary waves of the first kind in d dimensions," Phys. Rev. E **48**, 3998–4007 (1993).

29. S. Chávez Cerda, S. B. Cavalcanti, and J. M. Hickmann, "A variational approach of nonlinear dissipative pulse propagation," Eur. Phys. J. D **1**, 313–316 (1998).

30. F. Pedaci, P. Genevet, S. Barland, M. Giudici, and J. R. Tredicce, "Positioning cavity solitons with a phase mask," Appl. Phys. Lett. **89**, 221111 (2006).

31. A. J. Scroggie, J. M. McSloy, and W. J. Firth, "Self-propelled cavity solitons in semiconductor microcavities," Phys. Rev. E **66**, 036607 (2002).

32. T. Maggipinto, M. Brambilla, G. K. Harkness, and W. J. Firth, "Cavity solitons in semiconductor microresonators: Existence, stability, and dynamical properties," Phys. Rev. E **62**, 8726–8739 (2000).

33. Y. Menesguen, S. Barbay, X. Hachair, L. Leroy, I. Sagnes, and R. Kuszelewicz, "Optical self-organization and cavity solitons in optically pumped semiconductor microresonators," Phys. Rev. A **74**, 023818 (2006).

34. M. Tlidi, A. G. Vladimirov, D. Pieroux, and D. Turaev, "Spontaneous motion of cavity solitons induced by a delayed feedback," Phys. Rev. Lett. **103**, 103904 (2009).

35. F. Prati, L. A. Lugiato, G. Tissoni, and M. Brambilla, "Cavity soliton billiards," Phys. Rev. A **84**, 053852 (2011).

36. H. Vahed, R. Kheradmand, H. Tajalli, G. Tissoni, L. A. Lugiato, and F. Prati, "Phase-mediated long-range interactions of cavity solitons in a semiconductor laser with a saturable absorber," Phys. Rev. A **84**, 063814 (2011).

37. D. V. Skryabin and W. J. Firth, "Interaction of cavity solitons in degenerate optical parametric oscillators," Opt. Lett. **24**, 1056–1058 (1999).

38. S. V. Fedorov, A. G. Vladimirov, G. V. Khodova, and N. N. Rosanov, "Effect of frequency detunings and finite relaxation rates on laser localized structures," Phys. Rev. E **61**, 5814–5824 (2000).

39. K. Panajotov and M. Tlidi, "Chaotic behavior of cavity solitons induced by time delay feedback," Opt. Lett. **39**, 4739–4742 (2014).

40. N. Bekki and K. Nozaki, "Formations of spatial patterns and holes in the generalized ginzburg-landau equation," Phys. Lett. A **110**, 133 – 135 (1985).

41. P. Marcq, H. Chate, and R. Conte, "Exact solutions of the one-dimensional quintic complex ginzburg-landau equation," Physica D: Nonlinear Phenomena **73**, 305 – 317 (1994).

42. K. Pushkarov, D. Pushkarov, and I. Tomov, "Self-action of light beams in nonlinear media: soliton solutions," Opt. Quant. Electron. **11**, 471–478 (1979).

43. C. De Angelis, "Self-trapped propagation in the nonlinear cubic-quintic schrodinger equation: a variational approach," IEEE J. Quant. Electron. **30**, 818–821 (1994).